

# Geometrical frustration of an extended Hubbard diamond chain in the quasi-atomic limit

Onofre Rojas<sup>1</sup>, S. M. de Souza<sup>1</sup> and N. S. Ananikian<sup>1,2</sup>

<sup>1</sup>*Departamento de Ciências Exatas, Universidade Federal de Lavras, CP 3037, 37200-000, Lavras- MG, Brazil and*

<sup>2</sup>*A.I. Alikhanyan National Science Laboratory, 0036 Yerevan, Armenia.*

We study the geometrical frustration of extended Hubbard model on diamond chain, where vertical lines correspond to the hopping and repulsive Coulomb interaction terms between sites, while the rest of them represent only the Coulomb repulsion one. The phase diagrams at zero temperature show quite curious phases: five types of frustrated states and four types of non-frustrated ones, ordered antiferromagnetically. Although decoration transformation was derived to spin coupling systems, this approach can be applied to electron coupling ones. Thus the extended Hubbard model can be mapped onto another effective extended Hubbard model in atomic limit with additional three and four-body couplings. This effective model is solved exactly through transfer matrix method. In addition, using the exact solution of this model we discuss several thermodynamic properties away from half filled band, such as chemical potential behavior, electronic density, entropy, where we study the geometrical frustration, consequently we investigate the specific heat as well.

PACS numbers: 75.10.Lp, 71.10.Fd, 71.27.+a, 75.10.Jm, 31.10.+z

Keywords: Hubbard model; geometric frustration; Exact solution; Strongly correlated electron systems

## I. INTRODUCTION

The Hubbard model is one of the simplest model for strongly interacting electron systems. In general, rigorous analysis of the model is a difficult task, only in particular case a number of rigorous exact results have been obtained<sup>1</sup>. On the other hand, geometrical frustration in strongly correlated electron systems have attracted a great deal of interest over the past decades<sup>2,3</sup>. For instance, due to the competition between the nearest and the next-nearest exchange coupling, the inorganic spin-Peierls compound exhibits a transition from a gapless phase to a gaped dimerized ground state<sup>4</sup>. The quantum phase transition point from the gapless phase to the gaped dimerized phase of this model was first determined by Okamoto and Nomura<sup>5</sup>.

The interplay between geometrical frustration and strong electron correlation results in a complicated phase diagram, containing many interesting phases: spin-gaped metallic phase, disorder magnetic insulation phase, Heisenberg insulator<sup>6</sup>. The Hubbard model on the triangular lattice shows a transition from a paramagnetic metal to an antiferromagnetic insulator as the Hubbard on-site repulsion gradually grows<sup>7</sup>.

Using the numerical diagonalization of finite size system Hida predicted the appearance of the magnetization plateau in one of the pioneering theoretical papers<sup>8</sup>. In the framework of the transfer-matrix and dynamical recursive approaches the frustrated magnetization plateaus were obtained for ferromagnetic-ferromagnetic-antiferromagnetic, kagome chains as well as zigzag ladder with multi-spin exchanges<sup>9-11</sup>.

For small nanoclusters by the exact numerical diagonalization the average electron density, magnetization plateaus via chemical potential or magnetic field have been studied in Hubbard model<sup>12,13</sup>.

Recently geometrical frustration of Hubbard model

was widely studied, particularly the diamond chain structure such as considered by Derzhko et al.<sup>14,15</sup>, where they discuss the frustration for a special class of lattice. Montenegro-Filho and Coutinho-Filho<sup>16</sup> also considered the doped  $AB_2$  Hubbard chain, both in the weak coupling and the infinite- $U$  limit (atomic limit). They studied a quite interesting phases as a function of hole doping away from half-filled band. Mancini<sup>17,18</sup> has presented the exact solution of extended one-dimensional Hubbard model in the atomic limit, obtaining the chemical potential plateaus of the particle density, of the on-site potential at zero temperature and studied the thermodynamic charge susceptibility, compressibility at finite temperature, as well as other physical quantities. Vidal et al.<sup>19</sup> also discussed two interacting particles evolving in a diamond chain structure embedded in a magnetic field. As the particles interact, it leads to the strong localization induced by the magnetic field for the particular value of a flux. Analogous model was also studied by Rossler and Mainemer<sup>20</sup>. The Hubbard model in other quasi-one-dimensional triangular structure also was studied by Wang<sup>21</sup>. The latter indicated that for small hopping term, the system exhibits short range antiferromagnetic correlation, whereas, when the hopping terms become greater than critical point, there is a transition from an antiferromagnetic state to a frustrated one. Moreover, the insulator-metal transition takes place at hopping interaction even greater than another critical point. Further Gulacsi et al.<sup>22,23</sup> also discussed the diamond Hubbard chain in a magnetic field and a wide range of properties such as flat-band ferromagnetism and correlation-induced metallic, half-metallic process. The spinless versions of the Hubbard model on diamond chain was also recently investigated through exact analytical solution<sup>24</sup>, as well as Lopes and Dias<sup>25</sup> performed a detailed investigation using the exact diagonalization approach.

In the last decade several diamond chain structures

were discussed. Some of them were motivated by real materials such as  $\text{Cu}_3(\text{CO}_3)_2(\text{OH})_2$  known as azurite, which is an interesting quantum antiferromagnetic model, described by Heisenberg model on generalized diamond chain. Honecker et al.<sup>26</sup> studied the dynamic and thermodynamic properties for this model. Besides, Pereira et al.<sup>27</sup> investigate the magnetization plateau of delocalized interstitial spins on diamond chain, as well as they detect magnetocaloric effect in kinetically frustrated diamond chain<sup>28</sup>. Quite recently, Lisnii<sup>29</sup> studied a distorted diamond Ising-Hubbard chain and that model exhibits geometrical frustration also. A further investigation regarding the exact evidence for the spontaneous antiferromagnetic long-range order in the two-dimensional hybrid model of localized Ising spins and itinerant electrons was discussed by Strečka et al.<sup>30,31</sup>. Moreover, the thermodynamics of the Ising-Heisenberg model on diamond-like chain was widely discussed in references<sup>32-35</sup>, and also the thermal entanglement was considered by Ananikian et al.<sup>36</sup>.

On the other hand, the analytical exact solution is rather amazing, since the exact result is always useful to manipulate against the numerical results. Therefore, the exact solutions of the models are of great importance, so our main goal is to obtain an exact solution for the extended Hubbard model on diamond chain in quasi-atomic limit. The research of the extended Hubbard diamond chain model without the hopping of electrons between the nodal sites is based on the three main reasons. First of all 1/3 magnetization plateau, the double peaks both in the magnetic susceptibility and specific heat was observed in the experimental measurements<sup>37,38</sup> according to the experiments of the natural mineral azurite. Theoretical calculations of the one-dimensional Hubbard model, as well as the experimental result of the exchange dimer (interstitial sites) parameter and their descriptions of the various theoretical models are presented. It should be noted that the dimers (interstitial sites) exchange much more strongly than those nodal sites. There were proposed various types of theoretical Heisenberg approximate methods: the renormalization of the density matrix renormalization group of the transfer matrix, the density functional theory, the high temperature expansion, Lanczos diagonalization on a diamond chain are to explain the experimental measurements (magnetization plateau and the double top) in natural mineral azurite<sup>39</sup>. All of these theoretical studies are approximate. There is another possibility. Since dimer interaction is much higher than the rest, it can be represented as an exactly solvable Ising-Heisenberg model. In addition, experimental data on the magnetization plateau coincide with the approximation of Ising-Heisenberg model<sup>27,32,36,40</sup> and the extended Hubbard model without the hopping of electrons between the nodal sites<sup>24</sup> on a diamond chain. This is the first reason.

The second one is the quantum block-block entanglement, carried out by exact diagonalization technique in one-dimensional extended Hubbard model, calculated

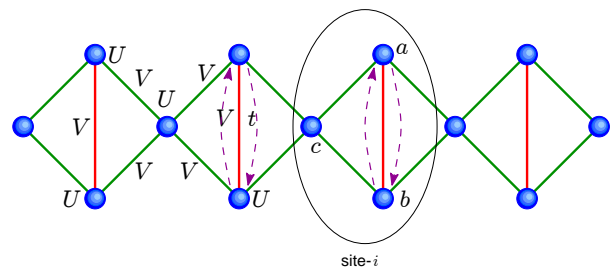


Figure 1: (Color online) Schematic representation of extended Hubbard model on diamond chain.

for finite size ( $L=10$ )<sup>41</sup>. When the absolute value of nearest-neighbor Coulomb interactions (our case) becomes smaller, the effect of the hopping term and the onsite interaction cannot be neglected. Finally, we would like to point out that although the results, obtained in this paper are for the 2-site (dimer) system, their qualitative features are the same as for big size system ones.

And, the third reason is the experimental observation of the double peaks both in the magnetic susceptibility and specific heat<sup>27,39,42</sup> may be described exactly by the extended Hubbard diamond chain model without the hopping of electrons or holes between the nodal sites. This phenomenon is particularly important in the quantum case.

This paper is organized as follows: in Sec. II we present the extended Hubbard model on diamond chain. We have studied the phase diagram at zero temperature in Sec. III. Further, in Sec. IV, we present the exact solution of the model. In Sec. V, we have discussed the thermodynamic properties of the model, such as electronic density, internal energy, compressibility, entropy and specific heat away from the half-filled band. Finally, Sec. VI contains the concluding remarks.

## II. THE EXTENDED HUBBARD MODEL

The extended Hubbard model on diamond chain will be considered in this paper, as represented schematically in FIG. 1. In the present model we consider the hopping term  $t$  between sites  $a$  and  $b$ , besides, there are onsite Coulomb repulsion interaction term denoted by  $U$  and the nearest neighbor repulsion interaction term, denoted by  $V$ . We assume also that this model has an arbitrary particle density, so, we will include a chemical potential term noted by  $\mu$ , therefore the Hamiltonian of this model can be expressed by:

$$\mathbf{H} = \sum_{i=1}^N \mathbf{H}_{i,i+1}, \quad (1)$$

with  $N$  being the number of cell (sites  $a$ ,  $b$  and  $c$ ), whereas  $\mathbf{H}_{i,i+1}$  is given by

$$\begin{aligned}
\mathbf{H}_{i,i+1} = & -t \sum_{\sigma=\downarrow,\uparrow} \left( \mathbf{a}_{i,\sigma}^\dagger \mathbf{b}_{i,\sigma} + \mathbf{a}_{i,\sigma} \mathbf{b}_{i,\sigma}^\dagger \right) - \\
& - \mu \left( \mathbf{n}_i^a + \mathbf{n}_i^b + \frac{1}{2}(\mathbf{n}_i^c + \mathbf{n}_{i+1}^c) \right) + \\
& + U \left( \mathbf{n}_{i,\uparrow}^a \mathbf{n}_{i,\downarrow}^a + \mathbf{n}_{i,\uparrow}^b \mathbf{n}_{i,\downarrow}^b + \frac{1}{2}(\mathbf{n}_{i,\uparrow}^c \mathbf{n}_{i,\downarrow}^c + \mathbf{n}_{i+1,\uparrow}^c \mathbf{n}_{i+1,\downarrow}^c) \right) + \\
& + V \left( \mathbf{n}_i^a \mathbf{n}_i^b + \frac{1}{2}(\mathbf{n}_i^a + \mathbf{n}_i^b)(\mathbf{n}_i^c + \mathbf{n}_{i+1}^c) \right), \quad (2)
\end{aligned}$$

with  $\mathbf{a}_{i,\sigma}$ , and  $\mathbf{b}_{i,\sigma}$  ( $\mathbf{a}_{i,\sigma}^\dagger$  and  $\mathbf{b}_{i,\sigma}^\dagger$ ) being the Fermi annihilation (creation) operator for the Hubbard model, while by  $\sigma$  we represent the electron spin, and by  $\mathbf{n}_{i,\sigma}^\alpha$  we mean the number operator, with  $\alpha = \{a, b, c\}$ , using this number operator we define also the following operators  $\mathbf{n}_i^\alpha = \mathbf{n}_{i,\uparrow}^\alpha + \mathbf{n}_{i,\downarrow}^\alpha$ .

In order to contract the Hamiltonian (2), we can define the following operators

$$\begin{aligned}
\mathbf{p}_{i,i+1} &= \frac{1}{2}(\mathbf{n}_i^c + \mathbf{n}_{i+1}^c), \\
\mathbf{q}_{i,i+1} &= \frac{1}{2}(\mathbf{n}_{i,\uparrow}^c \mathbf{n}_{i,\downarrow}^c + \mathbf{n}_{i+1,\uparrow}^c \mathbf{n}_{i+1,\downarrow}^c), \quad (3)
\end{aligned}$$

using these operators, we can rewrite the Hamiltonian (2), as follows:

$$\begin{aligned}
\mathbf{H}_{i,i+1} = & -t \sum_{\sigma=\downarrow,\uparrow} \left( \mathbf{a}_{i,\sigma}^\dagger \mathbf{b}_{i,\sigma} + \mathbf{a}_{i,\sigma} \mathbf{b}_{i,\sigma}^\dagger \right) - \\
& - (\mu - V \mathbf{p}_{i,i+1}) (\mathbf{n}_i^a + \mathbf{n}_i^b) + \\
& + U \left( \mathbf{n}_{i,\uparrow}^a \mathbf{n}_{i,\downarrow}^a + \mathbf{n}_{i,\uparrow}^b \mathbf{n}_{i,\downarrow}^b \right) + \\
& + V \mathbf{n}_i^a \mathbf{n}_i^b - \mu \mathbf{p}_{i,i+1} + U \mathbf{q}_{i,i+1}. \quad (4)
\end{aligned}$$

The symmetry particle-hole can be analyzed in a similar way, as discussed in reference<sup>24</sup>. The phase diagram in the half-filled band, can be obtained using the following restriction for the chemical potential  $\mu = U/2 + 2V$ . This relation could be obtained by using the symmetry particle-hole in a similar way, as discussed in reference<sup>24</sup>.

### III. THE PHASE DIAGRAM

In order to study the phase diagram at zero temperature, first we need to diagonalize the Hamiltonian (4) at sites  $a$  and  $b$ . Where by  $m = \{0, \dots, 4\}$  we will denote the total number of mobile electrons per unit cell at sites  $a$  and  $b$ , while by  $n_c$  we mean the number of electrons per unit cell at site- $c$ . The Hamiltonian at sites  $a$  and  $b$  can be written as  $16 \times 16$  matrix, but this matrix can be constructed as a block matrix, where in the largest block matrix we have  $4 \times 4$ , therefore the eigenvalues and eigenvectors of this matrix are expressed below as:

(a) State with  $m = 0$  particle

$$\lambda_0 = \mathbf{D}_0, \quad |S_0\rangle = |0, 0\rangle, \quad (5)$$

where  $\mathbf{D}_m = -(\mu - V \mathbf{p}_{i,i+1})m - \mu \mathbf{p}_{i,i+1} + U \mathbf{q}_{i,i+1}$ , While the state  $|S_0\rangle = |0, 0\rangle$  means there are no particle at site  $a$  and  $b$ , respectively.

(b) State with  $m = 1$  particle

$$\lambda_\sigma^{(\pm)} = \mathbf{D}_1 \pm t, \quad |S_\sigma^{(\pm)}\rangle = \frac{1}{\sqrt{2}} (|0, \sigma\rangle \mp |\sigma, 0\rangle), \quad (6)$$

with  $|S_\sigma^{(\pm)}\rangle$  we mean there is one particle at site  $a$  or  $b$  with either spin up or down.

(c) State with  $m = 2$  particles

$$\lambda_{2\sigma} = \mathbf{D}_2 + V, \quad |S_{2\sigma}\rangle = |\sigma, \sigma\rangle, \quad (7)$$

$$\lambda_{\uparrow\uparrow}^{(1)} = \mathbf{D}_2 + U, \quad |S_{\uparrow\uparrow}^{(1)}\rangle = \frac{1}{\sqrt{2}} (|\uparrow\uparrow, 0\rangle - |0, \uparrow\uparrow\rangle), \quad (8)$$

$$\lambda_{\uparrow\uparrow}^{(\pm)} = \mathbf{D}_2 + V + \frac{\theta_\pm t}{2}, \quad (9)$$

$$|S_{\uparrow\uparrow}^{(\pm)}\rangle = \frac{1}{\zeta_\mp} (|\uparrow\uparrow, 0\rangle + |0, \uparrow\uparrow\rangle + \theta_\mp (|\uparrow, \downarrow\rangle + |\downarrow, \uparrow\rangle)) \quad (10)$$

$$\lambda_{\uparrow\downarrow}^{(2)} = \mathbf{D}_2 + V, \quad |S_{\uparrow\downarrow}^{(2)}\rangle = \frac{1}{\sqrt{2}} (|\uparrow, \downarrow\rangle - |\downarrow, \uparrow\rangle), \quad (11)$$

where

$$\zeta_\pm = \sqrt{2 + \frac{\theta_\pm^2}{8}}, \quad (12)$$

$$\theta_\pm = \frac{U - V \pm \sqrt{(U - V)^2 + 16t^2}}{t}, \quad (13)$$

the states  $|S_{2\sigma}\rangle$  and  $|S_{\uparrow\uparrow}^{(\pm)}\rangle$  are defined in a similar way as defined in the previous case, two particles both with spin up or down and two particles with opposite spins.

(d) State with  $m = 3$  particles

$$\lambda_{\uparrow\uparrow\sigma}^{(\pm)} = \mathbf{D}_3 + U + 2V \pm t, \quad |S_{\uparrow\uparrow\sigma}^{(\pm)}\rangle = \frac{1}{\sqrt{2}} (|\uparrow\uparrow, \sigma\rangle \mp |\sigma, \uparrow\uparrow\rangle), \quad (14)$$

the states  $|S_{\uparrow\uparrow\sigma}^{(\pm)}\rangle$  correspond to two particles with opposite spin and one spin

(e) State with  $m = 4$  particles

$$\lambda_{\uparrow\uparrow\uparrow\uparrow} = \mathbf{D}_4 + 2U + 4V, \quad |S_{\uparrow\uparrow\uparrow\uparrow}\rangle = |\uparrow\uparrow, \uparrow\uparrow\rangle. \quad (15)$$

the state  $|S_{\uparrow\uparrow\uparrow\uparrow}\rangle$  means there are two spins at each site with opposite spins.

It is worth to note that, the Hamiltonian (2), has 256 eigenvalues per diamond plaquette.

From here after, we will consider only repulsive on-site Coulomb interaction ( $U > 0$ ) as well as repulsive Coulomb interaction between nearest neighbor ( $V > 0$ ). Besides  $V < U$ , in order to make more realistic our discussion.

Afterwards we will discuss the phase diagram at zero temperature, the present model exhibits 9 states which are tabulated in table I, for all possible numbers of particles available in the chain. For the empty particle and fully filled particles, we have one state  $|S_0\rangle = |\text{Vac}\rangle$  and  $|S_6\rangle = |\text{Full}\rangle$ , respectively. While for one particle per unit cell and five particles per unit cell, we also have one corresponding frustrated state  $|S_1\rangle = |\text{FRU}_1\rangle$

$n_t$	Ground state energy	Ground state
0	0	$ S_0\rangle =  \text{Vac}\rangle = \prod_i  S_{0i}\rangle \otimes  0\rangle_i$
1	$-\mu - t$	$ S_1\rangle =  \text{FRU}_1\rangle = \prod_i  S_{\sigma}^{(-)}\rangle_i \otimes  0\rangle_i$
2	$-2\mu + V + \frac{\theta-t}{2}$	$ S_2\rangle =  \text{AFM}_2\rangle = \prod_i  S_{\sigma}^{(-)}\rangle_i \otimes  0\rangle_i$
2	$-2\mu - t + V$	$ \bar{S}_2\rangle =  \text{FRU}_2\rangle = \prod_i  S_{\sigma}^{(-)}\rangle_i \otimes  1\rangle_i$
3	$-3\mu + 3V + \frac{\theta-t}{2}$	$ S_3\rangle =  \text{FRU}_3\rangle = \prod_i  S_{\uparrow}^{(-)}\rangle_i \otimes  1\rangle_i$
4	$-4\mu + 5V + U + \frac{\theta-t}{2}$	$ S_4\rangle =  \text{AFM}_4\rangle = \prod_i  S_{\uparrow}^{(-)}\rangle_i \otimes  2\rangle_i$
4	$-4\mu - t + 5V + U$	$ \bar{S}_4\rangle =  \text{FRU}_4\rangle = \prod_i  S_{\uparrow}^{(-)}\rangle_i \otimes  1\rangle_i$
5	$-5\mu + 8V + 2U - t$	$ S_5\rangle =  \text{FRU}_5\rangle = \prod_i  S_{\uparrow}^{(-)}\rangle_i \otimes  2\rangle_i$
6	$-6\mu + 12V + 3U$	$ S_6\rangle =  \text{Full}\rangle = \prod_i  S_{\uparrow\uparrow}\rangle_i \otimes  2\rangle_i$

Table I: The first column  $n_t$  represents the number of particles per unit cell, in the second and third column is tabulated the ground state energy per unit cell and its corresponding ground state respectively.

and  $|S_5\rangle = |\text{FRU}_5\rangle$ , respectively. However, for 2 particles per unit cell, we have two states, one configuration is an antiferromagnetic state ( $|S_2\rangle = |\text{AFM}_2\rangle$ ), whereas other configuration is a frustrated state ( $|\bar{S}_2\rangle = |\text{FRU}_2\rangle$ ). Due to particle-hole symmetry the analyze for the case of four particles (or two holes) becomes analogous for the case of two particles, hence, we have one antiferromagnetically ordered state ( $|S_4\rangle = |\text{AFM}_4\rangle$ ) and another frustrated state ( $|\bar{S}_4\rangle = |\text{FRU}_4\rangle$ ). Furthermore, for the special case of half-filled particles (with 3 particles or holes per unit cell) we also could have two possible states, one frustrated state  $|S_3\rangle = |\text{FRU}_3\rangle$  and another antiferromagnetically ordered state ( $|S_3\rangle = |\text{AFM}_3\rangle$ ), however the case  $|\text{AFM}_3\rangle$  occurs only when  $V > U$ , this case we ignore, since, it is too artificial one. In FIG. 2 we illustrate the phase transition at zero temperature of these states. In FIG. 2(a) we illustrate the phase diagram of  $V/U$  versus  $\mu/U$ , for fixed value of  $t/U = 1$ , where we display seven states  $S_i$  ( $i = 0..6$ ). While in FIG. 2(b) we display the phase diagram of  $t/U$  versus  $\mu/U$ , for fixed value of  $V/U = 0.25$ . This phase diagram illustrates 9 states, the seven states are already shown in FIG. 2(a) and two additional ones  $|\text{FRU}_2\rangle$  and  $|\text{FRU}_4\rangle$ . The fully transition boundary functions between states are tabulated in table II. The first and third columns correspond to the boundary states, while the second and fourth columns correspond to the boundary functions.

In FIG. 2, by dashed line we represent the half-filled band curve of the extended Hubbard model on diamond chain.

Other variants of the phase diagram at zero temperature could also be discussed, although the main properties already had been discussed in FIG. 2.

#### IV. EXACT SOLUTION

The method to be used will be the decoration transformation early proposed by Syozi<sup>43</sup> and Fisher<sup>44</sup>, more

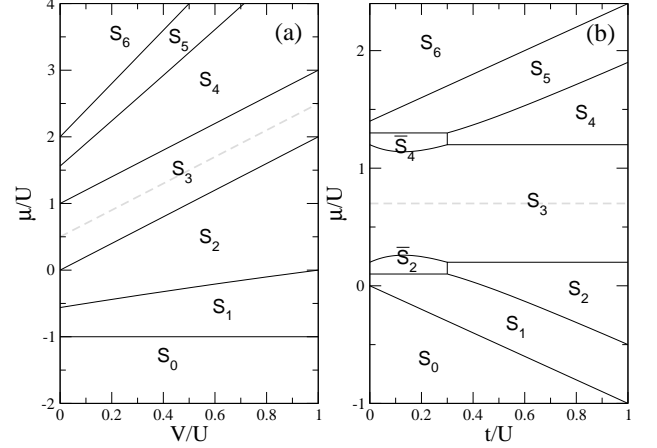


Figure 2: Phase diagrams at zero temperature: (a) displays the phase diagram of  $V/U$  versus  $\mu/U$  for fixed value of  $t/U = 1$ . Whereas in (b) displays the phase diagram of  $t/U$  versus  $\mu/U$  for fixed value of  $V/U = 0.25$ .

State	$V' \times \mu/U$ (fig. 2a)	State	$t' \times \mu/U$ (fig. 2b)
$S_0, S_1$	-1	$S_0, S_1$	$-t'$
$S_1, S_2$	$\frac{3+V'-\sqrt{(V'-1)^2+16}}{2}$	$S_1, S_2$	$\frac{11-10\sqrt{0.81+16t'^2}+20t'}{20}$
$S_2, S_3$	$2V'$	$S_2, S_3$	$\frac{1}{5}$
$S_3, S_4$	$2V' + 1$	$S_3, S_4$	$\frac{6}{5}$
$S_4, S_5$	$\frac{-1+7V'-\sqrt{(V'-1)^2+16}}{2}$	$S_4, S_5$	$\frac{17-20t'+5\sqrt{0.81+16t'^2}}{20}$
$S_5, S_6$	$4V' + 2$	$S_5, S_6$	$t' + \frac{7}{5}$
		$S_5, \bar{S}_4$	$\frac{13}{10}$
		$\bar{S}_4, S_3$	$\frac{-4t'+3+2\sqrt{0.81+16t'^2}}{4}$
		$S_3, \bar{S}_2$	$\frac{20t'+13-10\sqrt{0.81+16t'^2}}{20}$
		$\bar{S}_2, S_1$	$\frac{1}{10}$

Table II: The first and third columns represent the boundary between two states tabulated in table I, while the second and fourth columns mean the function of boundaries. For simplicity we use the following notation  $V' = V/U$  and  $t' = t/U$

later this approach was the subject of study by Rojas et al.<sup>45</sup>, for the case of multi-spins. As well as by Strečka<sup>46</sup> for the hybrid system (e.g. Ising-Heisenberg). Another interesting variant of this approach is also discussed by us, where we propose a direct transformation instead of several step by step one<sup>47</sup>, an illustrative successful application of the last approach was performed in reference<sup>48</sup>. The decoration transformation approach is widely used to solve spin models, however the decoration transformation approach can also be applied to electron coupling system, such have been used by the authors<sup>24</sup>

for the case of spinless fermion on diamond structure.

Therefore, in order to use the decoration transformation approach we can write the Boltzmann factor for extended Hubbard model on diamond chain as follows:

$$w_{\mathbf{n}_i^c, \mathbf{n}_{i+1}^c} = e^{-\beta \mathbf{D}_0} + 4 \left( e^{-\beta \mathbf{D}_1} + e^{-\beta(\mathbf{D}_3 + U + 2V)} \right) \cosh(\beta t) \\ + e^{-\beta \mathbf{D}_2} \left( e^{-\beta U} + 3e^{-\beta V} \right) + e^{-\beta(\mathbf{D}_4 + 2U + 4V)} + \\ + e^{-\beta(\mathbf{D}_2 + V)} \left( e^{-\beta\theta + t/2} + e^{-\beta\theta - t/2} \right), \quad (16)$$

where the  $\theta_{\pm}$  already were defined in equation (13).

The extended Hubbard model on diamond chain can be mapped onto an effective extended Hubbard-like model in atomic limit, where it involves additional three-body and four-body interaction. Therefore, the effective extended Hubbard model becomes like:

$$\tilde{\mathbf{H}}_{i,i+1} = -\tilde{\mu} \mathbf{n}_i^c + \tilde{U} \mathbf{n}_{i,\uparrow}^c \mathbf{n}_{i,\downarrow}^c \\ + \tilde{V} \left( \mathbf{n}_{i,\uparrow}^c + \mathbf{n}_{i,\downarrow}^c \right) \left( \mathbf{n}_{i+1,\uparrow}^c + \mathbf{n}_{i+1,\downarrow}^c \right) \\ + \tilde{W}_3 \mathbf{n}_{i,\uparrow}^c \mathbf{n}_{i,\downarrow}^c \left( \mathbf{n}_{i+1,\uparrow}^c + \mathbf{n}_{i+1,\downarrow}^c \right) \\ + \tilde{W}_4 \mathbf{n}_{i,\uparrow}^c \mathbf{n}_{i,\downarrow}^c \mathbf{n}_{i+1,\uparrow}^c \mathbf{n}_{i+1,\downarrow}^c, \quad (17)$$

where  $\tilde{\mu}$  could be interpreted as effective chemical potential, in a similar way,  $\tilde{U}$  labels the onsite Coulomb repulsion coupling, meanwhile  $\tilde{V}$  corresponds to the nearest neighbor repulsion coupling, the next terms,  $\tilde{W}_3$  will be interpreted as three body interaction term, whereas  $\tilde{W}_4$  as four body coupling. All the above parameters could be obtained as a function of Hamiltonian (2) parameters, when decoration transformation is performed

The Boltzmann factor for effective Hubbard model in atomic limit becomes like:

$$\tilde{w}_{\mathbf{n}_i^c, \mathbf{n}_{i+1}^c} = A e^{-\beta \tilde{\mathbf{H}}_{i,i+1}}, \quad (18)$$

the factor  $A$  is an additional variable to be determined in terms of the original Hamiltonian (2). By the use of decoration transformation<sup>43-45</sup> we will impose the following condition

$$w_{\mathbf{n}_i^c, \mathbf{n}_{i+1}^c} = \tilde{w}_{\mathbf{n}_i^c, \mathbf{n}_{i+1}^c}, \quad (19)$$

using Eq. (19) we can find all parameters of the effective Hamiltonian (17) and the factor  $A$ .

To solve the effective Hubbard model with up to four-body coupling, we can use the transfer matrix method<sup>49</sup>, similarly to that used in reference<sup>24,50</sup>. Therefore we symmetrize the Hamiltonian by exchanging  $i \rightarrow i+1$  and  $i+1 \rightarrow i$ , thus, the transfer matrix becomes symmetric, for our case, this transfer matrix could be expressed by:

$$\mathbf{T} = \begin{bmatrix} w_{0,0} & w_{0,1} & w_{0,1} & w_{0,2} \\ w_{0,1} & w_{1,1} & w_{1,1} & w_{1,2} \\ w_{0,1} & w_{1,1} & w_{1,1} & w_{1,2} \\ w_{0,2} & w_{1,2} & w_{1,2} & w_{2,2} \end{bmatrix}, \quad (20)$$

where the Boltzmann factor is given by Eq. (16), and using a convenient notation, such as

$$w_{0,0}(x) = 1 + 2x \left( 1 + \frac{x^2}{z^4 y^2} \right) \left( \frac{1}{\gamma^2} + \gamma^2 \right) + \\ + x^2 \left( \frac{3}{z^2} + \frac{1}{y^2} + \frac{1}{yz\varsigma} + \frac{\varsigma}{yz} \right) + \frac{x^4}{y^4 z^8}, \quad (21)$$

with  $x = e^{2\beta\mu}$ ,  $y = e^{\frac{1}{2}\beta U}$ ,  $z = e^{\frac{1}{2}\beta V}$ ,  $\gamma = e^{\frac{1}{2}\beta t}$  and  $\varsigma = e^{\frac{1}{2}\beta\sqrt{(U-V)^2 + 16t^2}}$ . Whereas the remaining Boltzmann factors could be expressed easily through the function  $w_{0,0}(x)$  defined in Eq. (21) as follows:

$$w_{n_1, n_2}(x) = \frac{x^{(n_1+n_2)/2}}{y^{[n_1/2] + [n_2/2]}} w_{0,0} \left( \frac{x}{z^{n_1+n_2}} \right), \quad (22)$$

by [...] inside braces we mean the least integer of any real number. Thereafter, all elements of matrix (20) are well expressed just in terms of  $w_{0,0}(x)$ .

The Boltzmann factors for the effective Hubbard model (18) with three and four-body terms are given by:

$$\tilde{w}_{0,0} = A, \\ \tilde{w}_{0,1} = Ar; \quad r = e^{\beta\tilde{\mu}/2}, \\ \tilde{w}_{0,2} = Ars; \quad s = e^{-\beta\tilde{U}/2}, \\ \tilde{w}_{1,1} = Ar^2 t; \quad t = e^{-\beta\tilde{V}}, \\ \tilde{w}_{1,2} = Ar^3 s t^2 u; \quad u = e^{-\beta\tilde{W}_3/2}, \\ \tilde{w}_{2,2} = Ar^4 s^2 t^4 u^4 v. \quad (23)$$

The determinant of transfer matrix becomes a quartic equation of the form  $\det(\mathbf{T} - \Lambda) = \Lambda^4 + a_3 \Lambda^3 + a_2 \Lambda^2 + a_1 \Lambda$ , where the coefficients become:

$$a_1 = -2w_{0,0}w_{1,1}w_{2,2} + 2w_{0,2}^2 w_{1,1} + 2w_{0,1}^2 w_{2,2} + \\ + 2w_{0,0}w_{1,2}^2 - 4w_{0,2}w_{0,1}w_{1,2}, \\ a_2 = -2w_{0,1}^2 + 2w_{0,0}w_{1,1} + w_{0,0}w_{2,2} + \\ + 2w_{1,1}w_{2,2} - w_{0,2}^2 - 2w_{1,2}^2, \\ a_3 = -w_{0,0} - w_{2,2} - 2w_{1,1}, \quad (24)$$

or alternatively the coefficients also can be expressed, using the effective Hamiltonian parameters, thus, the coefficients of the quartic equation are given by:

$$a_1 = A \left( -2r^6 t^5 s^2 u^4 v + 2r^6 s^2 t + 2r^6 s^2 t^4 u^4 v + \\ + 2r^6 s^2 t^4 u^2 - 4r^6 s^2 t^2 u \right), \\ a_2 = A \left( -2r^2 + 2r^2 t + r^4 s^2 t^4 u^4 v + 2r^6 t^5 s^2 u^4 v - \\ - r^4 s^2 - 2r^6 s^2 t^4 u^2 \right), \\ a_3 = -A \left( 1 + r^4 s^2 t^4 u^4 v + 2r^2 t \right). \quad (25)$$

Therefore the roots of algebraic quartic equation may be reduced to a cubic one, solutions of which are given in the following way:

$$\Lambda_j = 2\sqrt{Q} \cos \left( \frac{\phi + 2\pi j}{3} \right) - \frac{1}{3} a_3 \quad j = 0, 1, 2, \quad (26)$$

with

$$\begin{aligned}\phi &= \arccos\left(\frac{R}{\sqrt{Q^3}}\right), \\ Q &= \frac{a_3^2 - 3a_2}{9}, \\ R &= \frac{9a_2a_3 - 27a_1 - 2a_3^3}{54}.\end{aligned}\quad (27)$$

Furthermore, we also have additional trivial solution  $\Lambda_3 = 0$ , of the algebraic quartic equation.

Hence, the largest eigenvalue of the transfer matrix will be  $\Lambda_0$ , which is expressed by Eq. (26). Once known the largest eigenvalue of transfer matrix, we are able to obtain the partition function straightforwardly, and thereafter the free energy is given by  $f = -\frac{1}{\beta} \ln(\Lambda_0)$ . Using the free energy per unit cell, we may obtain the thermodynamic properties and how the model behaves when the number particles are changing away from the half filled band.

## V. THERMODYNAMIC PROPERTIES

In order to study the thermodynamic properties we will use the exact free energy  $f = -\frac{1}{\beta} \ln(\Lambda_0)$  as a starting point. Therefore, we will proceed our discussion of thermodynamic properties as a function of temperature, chemical potential and electronic density. Assuming that we are considering only repulsive onsite Coulomb interaction ( $U > 0$ ) as well as repulsive Coulomb interaction between nearest neighbor ( $V > 0$ ). Besides  $V < U$ , in order to make more realistic our discussion.

### A. The electronic density

We will explore the electronic density  $\rho = -\frac{\partial f}{\partial \mu}$ , as a function of chemical potential as well as the hopping term. In FIG. 3, we plot the chemical potential  $\mu/U$  versus  $t/U$ , for fixed value of temperature  $T/U = 0.01$  and nearest neighbor coupling  $V/U = 0.1$ . With gray scale, we mean electronic density between  $0 < \rho < 2$ , the darkest region corresponds to the lowest electronic density, while the brightest region corresponds to fully filled electrons.

In FIG. 4(a), we plot the electronic density as a function of chemical potential at low temperature for fixed value of hopping term  $t/U = 0.5$  and  $V/U = 0.1$ , showing six plateaus at  $\rho = 0, 1/3, 2/3, 1, 4/3, 5/3$  and 2, this phenomenon vanishes as soon as the temperature increases. Whereas in FIG. 4(b) we plot the same quantity but for large hopping term  $t/U = 2$  and  $V/U = 0.1$ . In this case the plateaus corresponding to electronic densities  $\rho = 1/3, 2/3, 4/3$  and  $5/3$ , which turn away from the half filled band  $\rho = 1$ . Moreover, the plateaus for

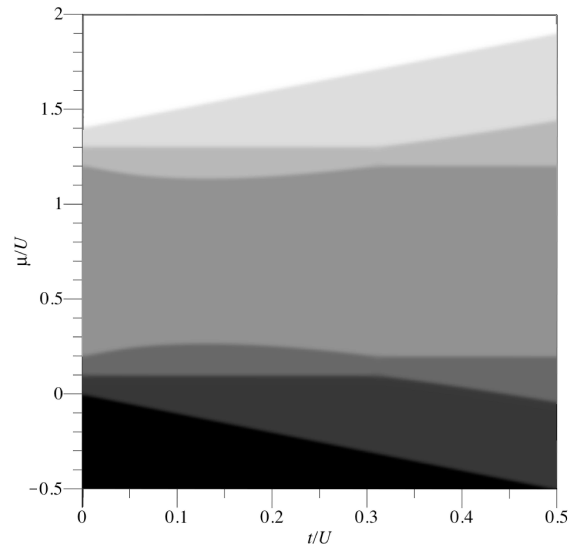


Figure 3: Electronic density per site for  $T/U = 0.01$  and  $V/U = 0.1$ , as a function of the  $t/U$  and  $\mu/U$ , where the black region corresponds to empty particles, while the white region corresponds to fully filled electrons or empty holes, by different levels of gray regions we represent the intermediate electronic density.

densities  $2/3$  and  $4/3$  become larger, as we can show in FIG. 4, which is also in agreement with FIG. 3.

### B. The internal energy

The internal energy  $\mathcal{E} = -\frac{\partial \ln(\Lambda_0)}{\partial \beta}$ , for extended Hubbard model will be discussed as a function of electronic density. In FIG. 5(a) the internal energy is plotted for small hopping term  $t/U = 0.2$  and  $V/U = 0.1$ , this internal energy exhibits a gap energy (step like function) at zero temperature, when the electronic density changes, but when temperature increases the step like function becomes smoother. Whereas in FIG. 5(b) for hopping term  $t/U = 0.5$  and  $V/U = 0.1$  is plotted and the shape of curves behaves basically similar plot to that  $t/U = 0.2$ . In summary, FIG. 5 displays the electronic density dependence as well as temperature dependence. We can see as far as the larger is the electronic density, the lower becomes the energy, although for low density around  $\rho = 0.5$  a maximum of internal energy. We also notice for several fixed values of temperature, the plot for the internal energy becomes smooth for sufficiently temperature.

### C. Compressibility

Another interesting amount that we could discuss will be the compressibility defined by  $\kappa(\rho) \equiv \frac{\partial \rho}{\partial \mu}$ ,

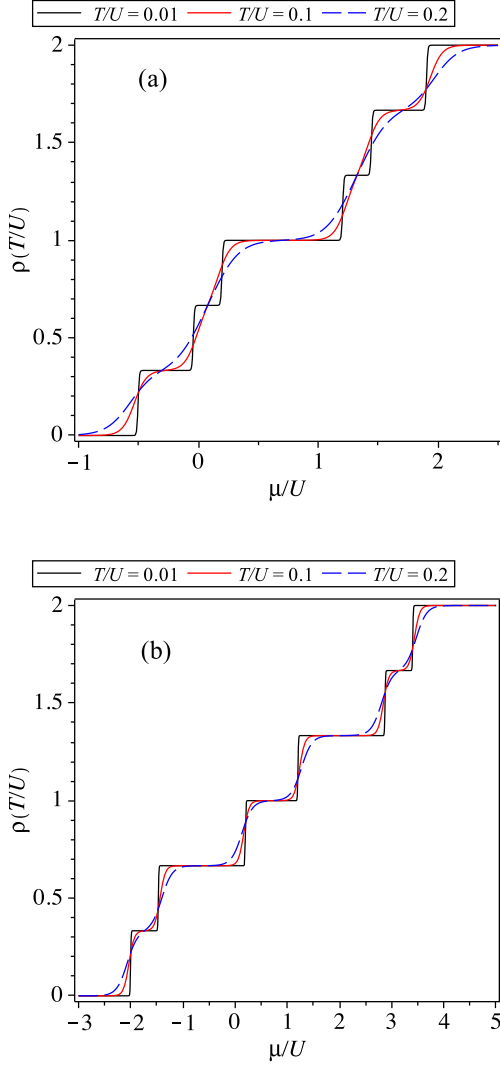


Figure 4: (Color online) Electronic density as a function of chemical potential, for fixed value of  $V/U = 0.1$ . (a) For  $t/U = 0.5$  and in (b) for  $t/U = 2.0$

which is convenient to study electron particles, instead of that compressibility sometimes known as total compressibility<sup>49</sup>  $\kappa_T = -\frac{1}{\rho^2} \frac{\partial^2 f}{\partial \mu^2} = \frac{\kappa}{\rho^2}$ . Therefore the compressibility will be discussed as a function of Hamiltonian parameters, temperature and electronic density. In FIG. 6 we display the compressibility behavior against the electronic density on the diamond chain, for fixed value of  $V/U = 0.1$ . In FIG. 6(a) we fixed the hopping term at  $t/U = 0.2$ , roughly below the phase transition occurs at  $t/U = 0.3$ , where we display how the compressibility behaves at low temperature. The compressibility becomes minimum (harder) close to the following fractional electronic densities, 0,  $1/3$ ,  $2/3$ , 1,  $4/3$ ,  $5/3$  and 2. Whereas there are 6 local maximum (softer) between fractional densities  $1/3$ ,  $2/3$ , 1,  $4/3$ ,  $5/3$  and 2, for temperature lower than  $T/U \lesssim 0.05$ . Whereas for

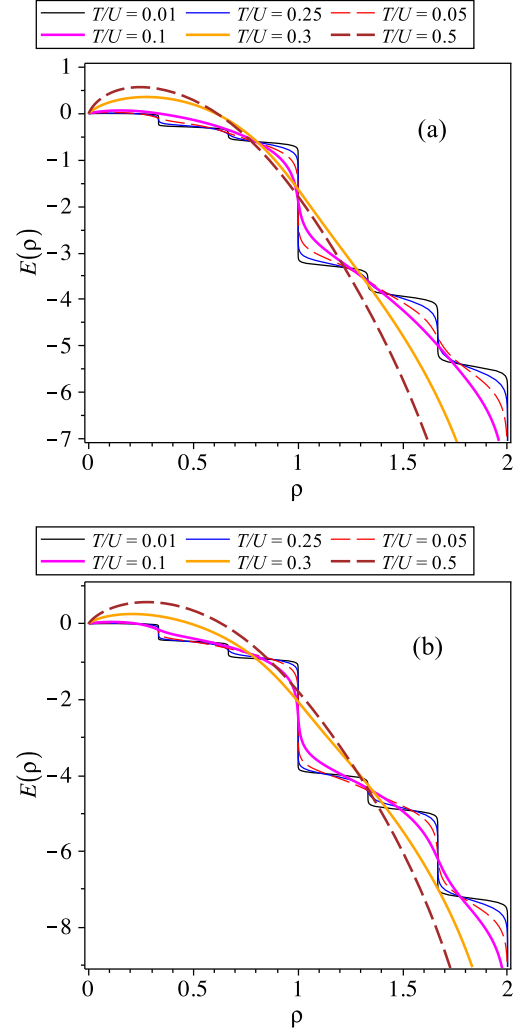


Figure 5: (Color online) Internal energy  $\mathcal{E}(\rho)$  as a function of electronic density  $\rho$  for given value of  $V/U = 0.1$ . (a) For  $t/U = 0.2$  and in (b) for  $t/U = 0.5$

$0.05 \lesssim T/U \lesssim 0.5$ , there is just one minimum at  $\rho = 1$ , besides the minimum at  $\rho = 0$  and  $\rho = 2$ . Furthermore, for higher temperature  $T/U \gtrsim 0.5$  the compressibility exhibits just one just one maximum at electronic density  $\rho = 1$ . In FIG. 6(b) we illustrate for  $t/U = 0.5$ , roughly above the phase transition. In principle, the behavior is quite similar to FIG. 6(a), a low compressibility survives for higher temperature  $t/U = 0.1$  at half filled band  $\rho = 1$ . Although, when temperature is sufficiently high ( $0.3 \lesssim T/U \lesssim 0.5$ ) there are only one minimum at  $\rho = 1$ , besides empty (fully) electrons, whereas for  $T/U \gtrsim 0.5$ , showing just a simple maximum at  $\rho = 1$ .

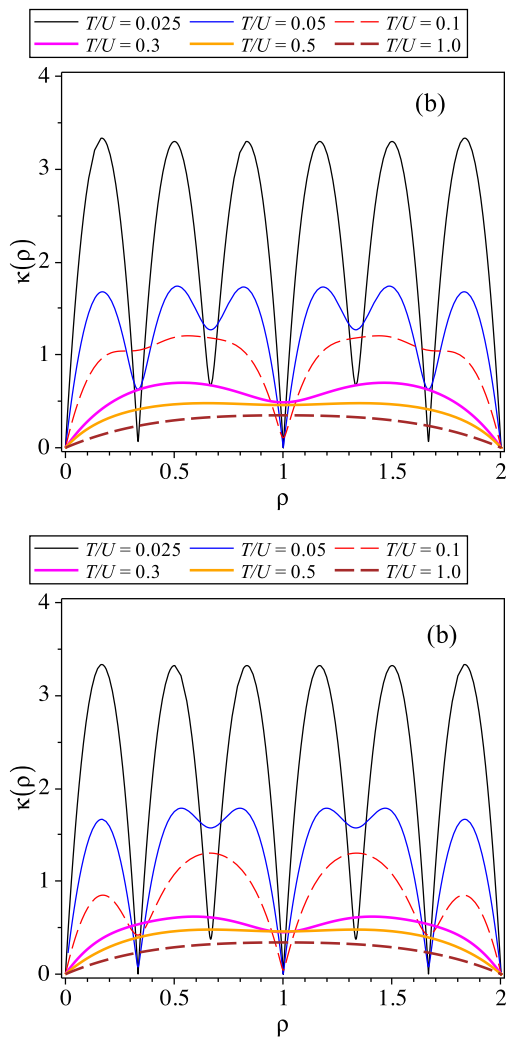


Figure 6: (Color online) The compressibility  $\kappa(\rho)$  as a function of electronic density  $\rho$ , for a fixed values of  $V/U = 0.1$ . (a) For  $t/U = 0.2$ , and in (b) for  $t/U = 0.5$ .

#### D. The entropy

Furthermore, we will study another interesting quantity the entropy  $\mathcal{S} = -\frac{\partial f}{\partial T}$ , and how the entropy behaves when the Hamiltonian parameters, temperature or even electronic density changes. In FIG. 7 we illustrate the magnitude of entropy, as a function of  $t/U$  and  $\mu/U$ , assuming a fixed value of  $V/U = 0.1$ . By different levels of gray scale, we represent the magnitude of entropy, the darkest region corresponds to lowest entropy while the brightest region corresponds to the higher entropy. At low temperature, the large value of entropy is related to the influence of the residual entropy. As far the temperature increases, the entropy curves become softer, as displayed in FIG. 7(a) for  $T/U = 0.01$  and in FIG. 7(b) for  $T/U = 0.05$ .

Mean while in FIG. 8, we display the entropy  $\mathcal{S}(\mu)$  as a

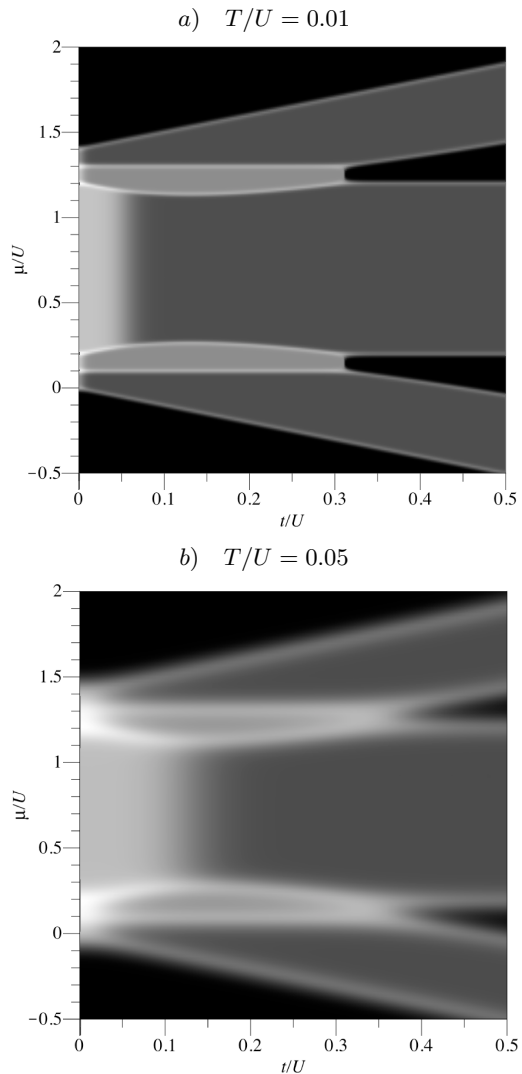


Figure 7: Entropy as a function of  $t/U$  and  $\mu/U$ , for fixed value of  $U/V = 0.1$ . Black region corresponds to non-frustrated entropy while the white region correspond to higher residual entropy effect, gray states correspond to intermediate residual entropy effect.

function of chemical potential, assuming a fixed value of  $V/U = 0.25$ , where we are able to illustrate the residual entropy effect, in agreement to FIG. 7.

The entropy indicates several peaks via the chemical potential. In FIG. 8(a) we plot for  $t/U = 0.2$  where is shown the influence of two types of residual entropy around of  $\mathcal{S} = \ln(2)$  and  $\ln(3)$ . Meanwhile, in FIG. 8(b) we display for  $t/U = 0.5$ . In this case we only display the influence of the residual entropy of  $\mathcal{S} = \ln(2)$ , certainly with the temperature increases we have the increase of entropy as well, however for large  $|\mu|$  the entropy is smaller than for small  $\mu \approx 1$ .

Whereas in FIG. 9, we display the entropy as a function of electronic density assuming a given parameter  $V/U = 0.1$ , for fixed value of parameter  $V/U = 0.1$ .

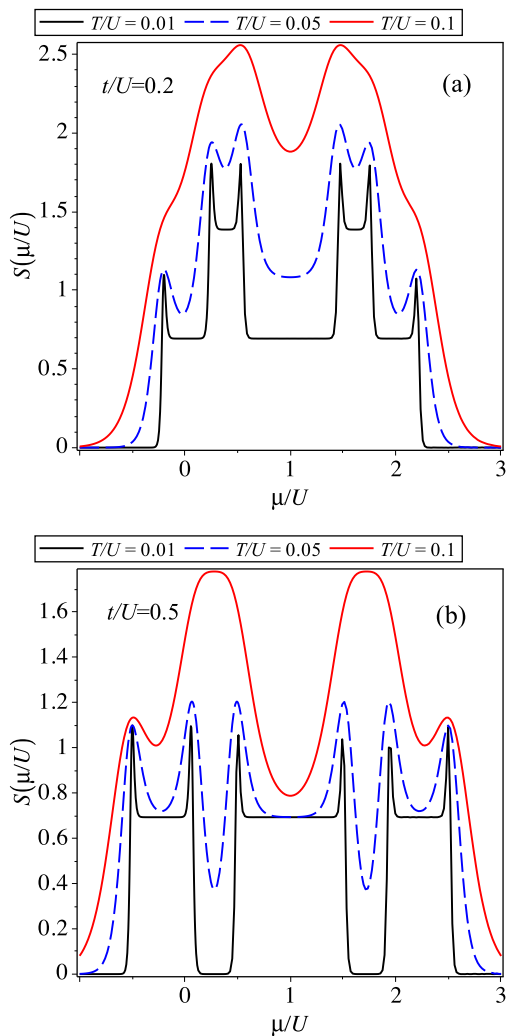


Figure 8: (Color online) Entropy  $S$  against  $\mu$  at low temperature assuming a fixed value of  $V/U = 0.25$ . (a) For  $t/U = 0.2$ , and in (b) for  $t/U = 0.5$

For high temperature  $T \geq 2$ , the entropy reaches its highest point at  $\rho = 1$ . We can note the residual entropy is strongly related to the electronic density. We also indicate, there is no residual entropy for a fully electronic density, therefore the entropy becomes lower even for high temperature.

For electronic density  $\rho = 1/3$  and  $2/3$  the residual entropy is  $S = \ln(2)$ , while for  $\rho = 4/3$  and  $5/3$  larger residual entropy is displayed  $S = \ln(4)$ .

### E. The specific heat

Finally we will discuss the specific heat  $C = -T \frac{\partial^2 f}{\partial T^2}$  behavior for extended Hubbard model in quasi-atomic limit. Thus, let us start displaying the specific heat as a function of chemical potential, which is illustrated in

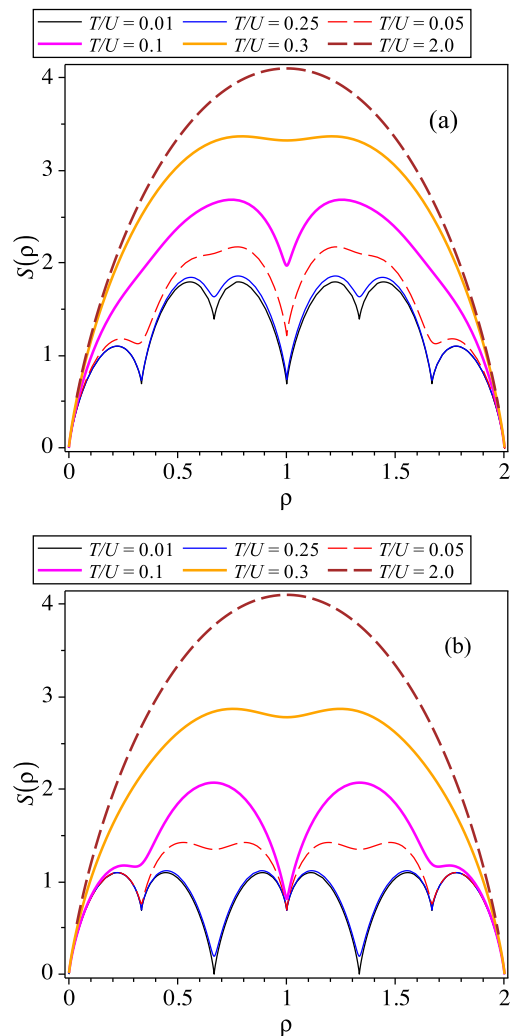


Figure 9: (Color online) Entropy against electronic density, assuming fixed Coulomb coupling  $V/U = 0.1$ . (a) For  $t/U = 0.2$ , and in (b) for  $t/U = 0.5$ .

FIG. 10 considering a fixed value of  $V/U = 0.25$ . In the low temperature limit, we can see the effect of the phase transition at zero temperature with very sharp peaks when the temperature decreases. Particularly, in FIG. 10(a) we display the specific heat as a function of  $\mu/U$  for  $t/U = 0.2$  while in (b) the specific heat as a function of  $\mu/U$  is illustrated for  $t/U = 0.5$ .

Lastly in FIG. 11 we display the specific heat as a function of temperature assuming the nearest neighbor Coulomb interaction  $V/U = 0.25$ . In FIG. 11(a) we consider for  $t/U = 0.2$ , while in FIG. 11(b) we assume for  $t/U = 0.5$ . From where we can see very sharp peaks as the temperature decreases, this anomalous peaks appears due to low lying energy around first order phase transition at zero temperature.

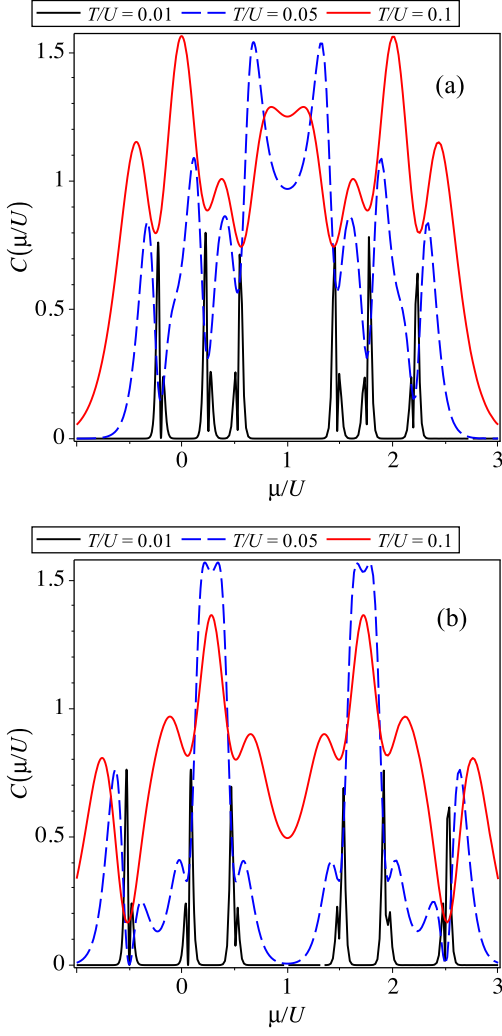


Figure 10: (Coloronline) The specific heat against chemical potential for low temperature, for a fixed value of  $V/U = 0.25$ . (a) For  $t/U = 0.2$ , and in (b) for  $t/U = 0.5$

## VI. CONCLUSIONS

The proposed Hubbard model on diamond chain, was discussed at zero temperature as well as at finite temperature. The phase diagram at zero temperature displays 4 frustrated states and 5 non-frustrated states antiferromagnetically ordered. Concerning to finite temperature properties, this model can be solved exactly through decoration transformation<sup>43–45,47</sup>. Transfer matrix technique<sup>49</sup> presents mapping the proposed model onto an exactly Hubbard model in atomic limit with three and four body couplings. Therefore, detailed thermodynamic properties were discussed, such as density as a function of chemical potential, illustrating 6 plateaus. Internal energy was also considered as function of electronic density far away from the half filled band, showing for several fixed temperatures. Besides we studied the

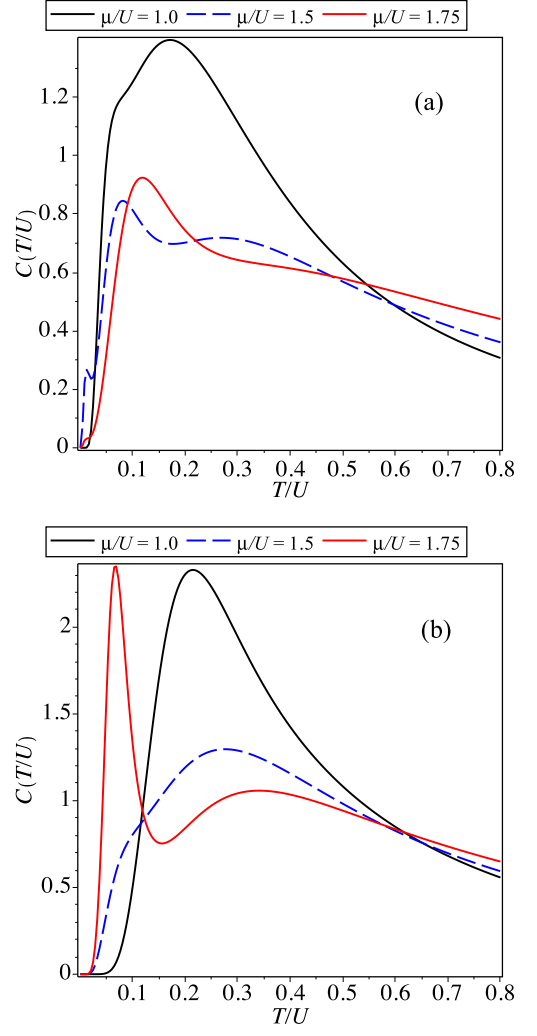


Figure 11: (Coloronline) The specific heat versus temperature, for a given value of  $V/U = 0.25$  and different values of chemical potential. In (a) is considered for  $t/U = 0.2$ , while in (b) for  $t/U = 0.5$ .

compressibility. Once again we illustrate this amount as a function of electronic density, and so we can conclude that the diamond chain is more compressible at low temperature, when the electronic density is respectively between  $1/3$ ,  $2/3$ ,  $1$ ,  $4/3$ ,  $5/3$ . As soon as the temperature increases, the compressibility decreases, turning into a simple decreasing curve as a function of density. We also considered the entropy as another interesting amount. This amount was studied as a function of chemical potential as well as electronic density, where we clearly observe the residual entropy contribution, owing to geometric frustration. Finally we discuss the specific heat, as a function of chemical potential and the temperature. In the nearest future, we plan to study the Coulomb interaction between the nodal (the monomer-monomer) sites and a different type of interaction between the nodal-interstitial (dimer-monomer) sites, both positive or neg-

ative ones, at the quantum level, which explains the wide range of experiments on the diamond chain.

### Acknowledgment

O. R. and de Souza thanks CNPq and Fapemig for partial financial support. This work has been supported

by the French-Armenian grant No. CNRS IE-017 (N.A.) and by the Brazilian FAPEMIG grant No. CEX à BPV à 00028-11 (N. A.).

- 
- <sup>1</sup> B. Nachtergaele, J. P. Solovej, J. Yngvason, *Condensed Matter Physics and Exactly Soluble Models*, Selecta of E. H. Lieb, (Springer, Berlin-Heidelberg, 2004).
- <sup>2</sup> I. S. Hagemann et al., Phys. Rev. Lett. **86**, 894 (2001).
- <sup>3</sup> J. van Lierop, D. H. Ryan, Phys. Rev. Lett. **86**, 4390 (2001).
- <sup>4</sup> S. Eggert, Phys. Rev. B **54**, R9612 (1996).
- <sup>5</sup> Okamoto and Nomura, Phys. Lett. A **169**, 433 (1992).
- <sup>6</sup> N. Laflorencie, D. Poilblanc, Phys. Rev. Lett. **90**, 157202 (2003).
- <sup>7</sup> S. Daul, R. M. Noack, Phys. Rev. B **61**, 1646 (2000).
- <sup>8</sup> K. Hida, J. Phys. Soc. Jpn. **63**, 2359 (1994).
- <sup>9</sup> V. R. Ohanyan, N. S. Ananikian, Phys. Lett. A **307**, 76 (2003).
- <sup>10</sup> V. V. Hovhannisyan, N.S. Ananikian, Phys. Lett. A **372**, 3363 (2008).
- <sup>11</sup> N. Ananikian, L. Ananikyan, R. Artuso, H. Lazaryan, Phys. Lett. A **374**, 4084 (2010).
- <sup>12</sup> A. N. Kocharian, G. W. Fernando, K. Palandage, J. W. Davenport, Phys. Rev. B **74**, 024511 (2006).
- <sup>13</sup> A. N. Kocharian, G. W. Fernando, K. Palandage, T. Wang, J. W. Davenport, Phys. Lett. A **364**, 57 (2007).
- <sup>14</sup> O. Derzhko, A. Honecker, J. Richter, Phys. Rev. B **79**, 054403 (2009).
- <sup>15</sup> O. Derzhko, J. Richter, A. Honecker, M. Maksymenko, R. Moessner Phys. Rev. B **81**, 014421 (2010).
- <sup>16</sup> R. R. Montenegro-Filho, M.D. Coutinho-Filho, Phys. Rev. B **74**, 125117 (2006).
- <sup>17</sup> F. Mancini, Eur. Phys. J. B **47**, 527 (2005).
- <sup>18</sup> F. Mancini, F. P. Mancini Phys. Rev. E **77**, 061120 (2008).
- <sup>19</sup> J. Vidal, R. Mosseri, B. Doucot, Phys. Rev. Lett. **81**, 5888 (1998); J. Vidal et al., **85**, 3906 (2000); B. Doucot and J. Vidal, Phys. Rev. Lett. **88**, 227005 (2002).
- <sup>20</sup> J. Rössler, D. Mainemer, Cond. Matter Phys. **13**, 13704 (2010).
- <sup>21</sup> W. Z. Wang, Phys. Rev. B **72**, 125116 (2005).
- <sup>22</sup> Z. Gulácsi, A. Kampf, D. Vollhardt, Phys. Rev. Lett. **99**, 026404 (2007).
- <sup>23</sup> Z. Gulácsi, A. Kampf, and D. Vollhardt, Prog. Theor. Phys. Suppl. **176**, 1 (2008).
- <sup>24</sup> O. Rojas, S.M. de Souza, Phys. Lett. A **375**, 1295 (2011).
- <sup>25</sup> A. A. Lopes, R.G. Dias, Phys. Rev. B **84**, 085124 (2011).
- <sup>26</sup> A. Honecker, S. Hu, R. Peters J. Phys.: Condens. Matter **23**, 164211 (2011).
- <sup>27</sup> M. S. S. Pereira, F. A. B. F. de Moura, M. L. Lyra, Phys. Rev. B **77**, 024402 (2008).
- <sup>28</sup> M. S. S. Pereira, F. A. B. F. de Moura, M. L. Lyra, Phys. Rev. B **79**, 054427 (2009).
- <sup>29</sup> B. M. Lisnii, Low Temp. Phys. **37**, 296 (2011).
- <sup>30</sup> J. Strečka, A. Tanaka, L. Čanova, T. Verkholyak, Phys. Rev. B **80**, 174410 (2009).
- <sup>31</sup> J. Strečka, A. Tanaka, M. Jasčur Journal of Physics Conference Series **200**, 022059 (2010).
- <sup>32</sup> L. Čanova, J. Strečka, M. Jascur, J. Phys.: Condens. Matter **18**, 4967 (2006).
- <sup>33</sup> O. Rojas, S.M. de Souza, V. Ohanyan, M. Khurshudyan, Phys. Rev. B **83**, 094430 (2011).
- <sup>34</sup> J. S. Valverde, O. Rojas, S. M. de Souza, J. Phys. Condens. Matter **20**, 345208 (2008).
- <sup>35</sup> B. M. Lisnii, Ukrainian Journal of Physics **56**, 1237 (2011).
- <sup>36</sup> N. S. Ananikian, L. N. Ananikyan, L. A. Chakhmakhchyan and O. Rojas, arXiv:1110.6406.
- <sup>37</sup> K. C. Rule et al., Phys. Rev. Lett. **100**, 117202 (2008).
- <sup>38</sup> H. Kikuchi et al., Phys. Rev. Lett. **94**, 227201 (2005); H. Kikuchi et al., Prog. Theor. Phys. Suppl. **159**, 1 (2005).
- <sup>39</sup> A. Honecker and A. Lauchli, Phys. Rev. B **63**, 174407 (2001); H. Jeschke et al., Phys. Rev. Lett. **106**, 217201 (2011); J. Kang et al., J. Phys. Condens. Matter **21**, 392201(2009); K. Takano, K. Kubo and H. Sakamoto, J. Phys.: Condens. Matter **8**, 6405 (1996); K Takano, K. Kubo and H. Sakamoto, J. Phys.: Condens. Matter **15**, 5979 (2003).
- <sup>40</sup> L. Chakhmakhchyan, N. Ananikian, L. Ananikyan and C. Burdik, J. Phys. Conf. Series **343**, 012022 (2012).
- <sup>41</sup> Sh.-S. Deng, Sh.-J. Gu, and H.-Q. Lin, Phys. Rev. B **74**, 045103 (2006).
- <sup>42</sup> B. Gu and G. Su, Phys. Rev. B **75**, 174437 (2007); Kang et al., J. Phys. Condens. Matter **21**, 392201(2009); O. Derzhko and J. Richter, Eur. Phys. J. B **52**, (2006) 23; B. Gu and G. Su, Phys. Rev. Lett. **97**, 089701 (2006); H. Kikuchi et al., Phys. Rev. Lett. **97**, 089702 (2006).
- <sup>43</sup> I. Syozi, Prog. Theor. Phys. **6**, 341 (1951).
- <sup>44</sup> M. Fisher, Phys. Rev. **113**, 969 (1959).
- <sup>45</sup> O. Rojas, J. S. Valverde, S. M. de Souza, Physica A **388**, 1419 (2009).
- <sup>46</sup> J. Strečka, Phys. Lett. A **374**, 3718 (2010).
- <sup>47</sup> O. Rojas, S. M. de Souza, J. Phys. A: Math. Theor. **44**, 245001 (2011).
- <sup>48</sup> M. Rojas, O. Rojas, S.M. de Souza arXiv:1105.5130.
- <sup>49</sup> R. J. Baxter, *Exactly Solved Models in Statistical Mechanics*, (Academic Press, New York, 1982).
- <sup>50</sup> G. Beni, P. Pincus Phys. Rev. B **9**, 2963 (1974).